Published in final edited form as:
Nucl Med Biol. 2012 April ; 39(3): 377–387. doi:10.1016/j.nucmedbio.2011.10.004.

^{64}Cu-NO2A-RGD-Glu-6-Ahx-BBN(7-14)NH_2: a heterodimeric targeting vector for positron emission tomography imaging of prostate cancer

Andrew B. Jackson[a], **Prasant K. Nanda**[a], **Tammy L. Rold**[c], **Gary L. Sieckman**[c], **Ashley F. Szczodroski**[c], **Timothy J. Hoffman**[a,c,d], **Xiaoyuan Chen**[e], and **Charles J. Smith**[a,b,c,d,*]

[a]Department of Radiology, University of Missouri School of Medicine, Columbia, MO 65211, USA

[b]University of Missouri Research Reactor Center, University of Missouri, Columbia, MO 65211, USA

[c]Research Division, Harry S. Truman Memorial Veterans' Hospital, Columbia, MO 65201, USA

[d]Department of Internal Medicine, University of Missouri School of Medicine, Columbia, MO 65211, USA

[e]Laboratory of Molecular Imaging and Nanomedicine, National Institute of Biomedical Imaging and Bioengineering, National Institutes of Health, Bethesda, MD 20892, USA

Abstract

Introduction—The present study describes the design and development of a new heterodimeric RGD-bombesin (BBN) agonist peptide ligand for dual receptor targeting of the form ^{64}Cu-NO2A-RGD-Glu-6-Ahx-BBN(7-14)NH_2 in which Cu-64=a positron emitting radiometal; NO2A=1,4,7-triazacyclononane-1,4-diacetic acid; Glu=glutamic acid; 6-Ahx=6-aminohexanoic acid; RGD=the amino acid sequence [Arg-Gly-Asp], a nonregulatory peptide that has been used extensively to target $\alpha_v\beta_3$ receptors up-regulated on tumor cells and neovasculature; and BBN(7-14)NH_2=Gln-Trp-Ala-Val-Gly-His-Leu-Met-NH_2, an agonist analogue of bombesin peptide for specific targeting of the gastrin-releasing peptide receptor (GRPr).

Methods—RGD-Glu-6-Ahx-BBN(7-14)NH_2 was manually coupled with NOTA (1,4,7-triazacyclononane-1,4,7-triacetic acid), and the resulting conjugate was labeled with ^{64}Cu to yield ^{64}Cu-NO2A-RGD-Glu-6-Ahx-BBN(7-14)NH_2. Purification was achieved via reversed-phase high-performance liquid chromatography and characterization confirmed by electrospray ionization–mass spectrometry.

Results—Competitive displacement binding assays displayed single-digit nanomolar IC_{50} values showing very high binding affinities toward the GRPr for the new heterodimeric peptide analogues. In vivo biodistribution studies showed high uptake and retention of tumor-associated radioactivity in PC-3 tumor-bearing rodent models with little accumulation and retention in nontarget tissues. The radiolabeled conjugate also exhibited rapid urinary excretion and high tumor-to-background ratios. Micro-positron emission tomography (microPET) molecular imaging investigations produced high-quality, high-contrast images in PC-3 tumor-bearing mice 15 h postinjection.

Conclusions—Based on microPET imaging experiments that show high-quality, high-contrast images with virtually no residual gastrointestinal radioactivity, this new heterodimeric RGD-BBN

*Corresponding author. Department of Radiology, MU School of Medicine, One Hospital Drive, Columbia, MO 65211, USA. Tel.: +1 573 814 6000x53683; fax: +1 573 814 6551. smithcj@health.missouri.edu (C.J. Smith).

conjugate can be considered as a promising PET tracer candidate for the diagnosis of GRPr-positive tumors in human patients.

Keywords

^{64}Cu; RGD-BBN; Heterodimeric peptide; Gastrin-releasing peptide receptor (GRPr); Integrin $\alpha_v\beta_3$ receptor; Positron emission tomography (PET)

1. Introduction

Gastrin-releasing peptide receptors (GRPrs) are expressed in very high numbers on certain human cancers [1–10], including human prostate cancer, and have been targeted with monomeric radiolabeled bombesin (BBN) analogues for diagnosis and therapy. However, the clinical utility of monomeric radiolabeled peptides can be limited by a number of factors including receptor density, binding affinity and pharmacokinetics. For example, high-quality, high tumor-to-background positron emission tomography (PET) or single photon emission computed tomography images require a high degree of receptor expression on tumor cells as compared to normal, collateral tissue. The number of effective receptors may differ significantly during tumor development, resulting in drastically reduced uptake and retention of targeting vector, limiting the quality of the diagnostic image. Also, the binding affinity of monomeric peptides can be relatively low as compared to heterodimeric targeting vectors. Radiolabeled monomeric regulatory peptides may also be limited by pharmacokinetic considerations. For example, clearance properties and excretion rates of targeting vector may limit the diagnostic imaging utility of a specific monomeric probe. For these reasons, heterodimeric or multivalent regulatory peptide probes have recently become a new avenue for diagnostic molecular imaging of tumors expressing either single- or multi-targetable receptors.

The ability to target multiple receptor subtypes via a heterodimeric targeting radioligand provides impetus to investigate the dual targeting capacity for improved in vivo PET images of specific human cancers. The RGD sequence, part of a cyclic five-residue moiety abbreviated as c(RGDyK), has been shown to target $\alpha_v\beta_3$ receptors, which are moderately expressed on androgen-independent prostate cancer cells [11–16]. Liu and co-workers have recently reported the synthesis of heterodimeric regulatory peptide probes based on RGD/BBN conjugates for $\alpha_v\beta_3$ integrin/GRPr dual receptor imaging in which they focused on PC-3 tumor uptake in nude mice with Ga-68 or Cu-64 radiolabeled NO3A-RGD-BBN(7-14)NH_2, (NO3A=*p*-NCS-Bz-NOTA) where the RGD and BBN targeting motifs are linked by a glutamic acid unit [17–21]. In these studies, they observed improved retention of Cu-64 tracer in tumor at 20 h postinjection (p.i.) as compared to the monomeric BBN or RGD conjugates. For example, PC-3 tumor retention was 2.04±0.35, 0.44±0.39 and 0.55±0.32 percent injected dose per gram (%ID/g) for ^{64}Cu-NO3A-RGD-BBN(7-14)NH_2, ^{64}Cu-NO3A-BBN(7-14)NH_2 and ^{64}Cu-NO3A-RGD, respectively. However, significant retention of the peptide ^{64}Cu-heterodimer was also observed in the kidneys (1.87±0.41%ID/g, 20 h p.i.) [18]. For ex vivo molecular imaging procedures such as PET, it is essential to have accumulation and prolonged retention of conjugate in receptor-expressing tumor and lack of retention in collateral tissue to produce higher target-to-nontarget ratios and high-quality images. Kidney uptake and retention observed by Liu could be due to usage of trivalent *p*-NCS-Bz-NOTA chelator (trianionic) in which the overall charge of the conjugate is presumably −1. This could limit the utility of these conjugates to be used for PET imaging of neuroendocrine tumors of the abdomen. Furthermore, renal toxicity continues to be a major drawback for therapy-based peptide conjugates utilizing β-emitting radionuclides and may limit the therapeutic efficacy of ^{64}Cu/^{67}Cu-conjugates of this general type. In our previous study, uptake of

monomeric ^{64}Cu-NO2A-8-Aoc-BBN(7-14) NH_2 in normal kidney was significantly reduced as compared to the RGD/BBN conjugate proposed by Liu. For example, only 0.42±0.04%ID/g of ^{64}Cu-NO2A-8-Aoc-BBN(7-14)NH_2 remained in normal kidney at 24 h p.i. [8] ^{64}Cu-NO2A-8-Aoc-BBN(7-14)NH_2, however, utilizes dianionic NO2A chelator to stabilize the +2 charge on the metal center, producing neutral peptide conjugates that may overcome prolonged retention in renal tissue, even at 24 h p.i. Therefore, conjugation of dianionic/divalent NO2A chelator to RGD/BBN dual targeting vectors offers an alternative approach for producing kinetically inert ^{64}Cu-conjugates having reduced renal retention for imaging and possible treatment of neuroendocrine tumors.

In this study, we present the development of a new heterodimeric RGD-bombesin agonist of the form ^{64}Cu-NO2A-RGD-Glu-6-Ahx-BBN(7-14)NH_2 in which ^{64}Cu=a positron emitting radiometal; NO2A=1,4,7-triazacyclononane-1,4-diacetic acid; Glu=glutamic acid; 6-Ahx=6-aminohexanoic acid; RGD=the amino acid sequence [Arg-Gly-Asp], a nonregulatory peptide sequence that has been used extensively to target $\alpha_v\beta_3$ receptors up-regulated on tumor cells and neovasculature; and BBN(7-14)NH_2=Gln-Trp-Ala-Val-Gly-His-Leu-Met-NH_2, a peptide targeting vector having high affinity for receptors localized on the surface of human prostate cancer cells. Detailed in vitro and in vivo investigations of this PET radiolabeled peptide targeting vector in human prostate PC-3 tumor cells are described. The microPET molecular imaging studies of this new heterodimeric RGD-BBN conjugate are also reported.

2. Materials and methods

2.1. General

RGD-Glu-6-Ahx-BBN(7-14)NH_2 was purchased from EZBiolab (Carmel, IN, USA). EDC and NHS coupling reagents were purchased from Advanced Chemtech (Louisville, KY). All other reagents/solvents were purchased from Fisher Scientific (Pittsburgh, PA, USA), Sigma-Aldrich Chemical Company (St. Louis, MO, USA) or ACROS Organics (Geel, Belgium) and used without further purification. ^{125}I-[Tyr^4]-BBN and ^{125}I-Echistatin were purchased from Perkin-Elmer (Waltham, MA, USA). Copper radionuclide in the form of $^{64}CuCl_2$ in 0.1 M HCl solution was purchased from the University of Wisconsin-Madison Medical Physics Department, USA.

The peptide conjugate and both metallated complexes that are reported herein were purified using reversed-phase high-performance liquid chromatography (RP-HPLC) performed on an SCL-10A HPLC system (Shimadzu, Kyoto, Japan) employing a binary gradient system [solvent A=99.9% DI water with 0.1% trifluoroacetic acid (TFA); solvent B=acetonitrile containing 0.1% TFA]. Samples were observed using an in-line Shimadzu SPD-10A absorption detector (λ=280 nm) as well as an in-line EG&G Ortec NaI solid crystal scintillation detector (EG&G, Salem, MA, USA). EZStart software (7.4; Shimadzu) was used for data acquisition of both signals. An analytical C-18 reversed-phase column (Phenomenex, Belmont, CA, USA) maintained at 34°C was used to achieve purification of NO2A-RGD-Glu-6-Ahx-BBN(7-14)NH_2. Purification and labeling of the peptide took place by using a linear gradient of 25:75A/B to 35:65 A/B gradient over 15 min, followed by an additional 10 min at 5:95 A/B. Purified peptide conjugates were lyophilized on a CentriVap system (Labconco, Kansas City, MO, USA).

2.2. Chemistry

2.2.1. Conjugation of NOTA to RGD-Glu-6-Ahx-BBN(7-14) NH_2 heterodimeric agonist peptide—The chelating agent NOTA was manually conjugated to RGD-Glu-6-Ahx-BBN(7-14)NH_2 heterodimeric agonist peptide via an active ester to produce NO2A-

RGD-Glu-6-Ahx-BBN(7-14)NH_2, following a known procedure [8,22]. Briefly, 20 equivalents of NOTA (54 μmol, 16.5 mg) were dissolved in 500 μl of 2-[morpholino]ethanesulfonic acid (MES) buffer. Fifty equivalents of sulfo-NHS (*N*-hydroxysulfosuccinimide) (136 μmol, 30 mg) and 30 equivalents of EDC (1-ethyl-3-[3-dimethylaminopropyl]carbodiimide hydrochloride) (82 μmol, 15.7 mg) were dissolved in 100 μl of MES buffer separately and added to the NOTA solution to allow the formation of active ester. The pH was adjusted to 4.7, and the solution was stirred at ambient temperature for 15 min. Then, 3 mg (2.7 μmol) of peptide were dissolved in 0.1 M sodium phosphate buffer (pH=7.0) and added to the active ester MES buffer solution. The pH was adjusted to 7.4 using 10% NaOH solution, and the reaction mixture was allowed to stir overnight at ambient temperature. The NO2A conjugate was purified by RP-HPLC using an analytical C-18 column (250×4.6 mm, 5 μm). The formation of NO2A-RGD-Glu-6-Ahx-BBN(7-14)NH2 conjugate was confirmed by electrospray ionization–mass spectrometry (ESI/MS) data analysis (Table 1).

2.3. Radiochemistry

2.3.1. ^{nat}Cu and ^{64}Cu labeling—^{nat}Cu-NO2A-RGD-Glu-6-Ahx-BBN(7-14)NH_2 conjugate was synthesized by the addition of $^{nat}CuCl_2 \cdot 2H_2O$ in 0.05 N HCl (90 nmol) to a plastic tube containing purified NO2A-RGD-Glu-6-Ahx-BBN(7-14)NH_2 peptide conjugate (80 nmol) and 0.4 M ammonium acetate (250 μl). The pH of the reaction mixture was adjusted to ~7 by the addition of 1% NaOH then incubated for 1 h at 70°C. Ten millimolar diethylenetriaminepentaacetic acid (DTPA) solution (50 μl) was added to scavenge unbound metal. The cold metallated conjugate was purified by RP-HPLC and analyzed by ESI/MS. The pure product was obtained as a white powder. Similarly, ^{64}Cu-NO2A-RGD-Glu-6-Ahx-BBN(7-14)NH_2 conjugate was synthesized by adding $^{64}CuCl_2$ in 0.1 M HCl (9.15×10^{18} Bq/mol) to a plastic tube containing purified peptide conjugate (50 μg) and 0.4 M ammonium acetate (250 μl). The pH of the reaction mixture was adjusted to ~7 by the addition of 1% NaOH and then incubated for 1 h at 70°C. Ten millimolar DTPA solution (50 μl) was added to scavenge unbound radiometal. Finally, the radiolabeled conjugate was purified by RP-HPLC and collected into 1 mg/ml bovine serum albumin (BSA) (100 μl) and ascorbic acid (10 mg) stabilizing agent prior to in vitro and in vivo evaluation. Acetonitrile was removed under a steady stream of nitrogen followed by quality control via an analytical radiometric chromatographic profile to determine radio-chemical purity and stability.

2.4. In vitro assays

2.4.1. Serum stability—Upon RP-HPLC purification, the ^{64}Cu-NO2A-RGD-Glu-6-Ahx-BBN(7-14)NH_2 conjugate was added to 500 μl of human serum albumin (HSA) (1 g/ml) in a small sample vial. Serum samples (pH 7.0±0.5) were incubated (37°C, 5% CO_2-enriched atmosphere) for 0, 1, 4 and 24 h. At each time point, the amount of ^{64}Cu dissociation from the NOTA ligand was assessed by RP-HPLC after serum proteins were removed via filtration through a 0.45-μm Millex-HV syringe filter (Millipore). HSA-associated radioactivity was also evaluated by counting the radioactivity prior to loading and after elution of the filter.

2.4.2. In vitro cell binding affinity studies—A competitive displacement binding assay was used to assess the binding affinity of NO2A-RGD-Glu-6-Ahx-BBN(7-14)NH_2 and ^{nat}Cu-NO2A-RGD-Glu-6-Ahx-BBN(7-14)NH_2 using PC-3 human prostate cancer cells and ^{125}I-[Tyr^4]-BBN as the displacement radioligand. Approximately 3×10^4 PC-3 cells (in D-MEM/F12K media containing 0.01M MEM (Minimum Essential Media) and 2% BSA, pH=5.5) were incubated with 20,000 counts per min of ^{125}I-[Tyr^4]-BBN (2.7×10^{-11} mol, 3.18×10^{17} Bq/mol) and increasing concentrations of metallated and nonmetallated heterodimeric RGD-BBN conjugates at 37°C (5% CO_2-enriched atmosphere) for 1 h. After

incubation, the reaction medium was aspirated, and the cells were washed four times with cold media. Cell-associated radioactivity was determined by counting the washed cells in a Packard Riastar multiwell gamma counting system. The percentage of ^{125}I-[Tyr^4]-BBN bound to the cells was plotted versus the concentration of metallated and nonmetallated RGD-BBN conjugates to determine the respective inhibitory concentration 50% (IC_{50}) values. The study was carried out in triplicate, and the final IC_{50} value was calculated by averaging the three experiments.

2.4.3. In vitro internalization assays—Internalization assays were determined in duplicate by incubating 3×10^4 PC-3 cells (in D-MEM/F12K media containing 0.01 M MEM and 2% BSA, pH=5.5) in the presence of 20,000 counts per min of ^{64}Cu-NO2A-RGD-Glu-6-Ahx-BBN(7-14)NH_2 (3.03×10^{-13} mol, 3.64×10^{19} Bq/mol) (37°C, 5% CO_2-enriched atmosphere). At 10, 20, 30, 45, 60, 90 and 120 min postincubation, the cells were aspirated, washed with fresh media and acetic acid/saline (pH=2.5, 4°C) to remove surface-bound radioactivity, and counted on a Packard Riastar gamma counter. Internalization was calculated relative to the total amount of activity added to the sample plate.

2.5. In vivo assays

2.5.1. Pharmacokinetic studies—All animal studies were conducted in compliance with the highest standards of care as outlined in the National Institutes of Health's *Guide for the Care and Use of Laboratory Animals* and the Policy and Procedures for Animal Research at the Harry S. Truman Memorial Veterans' Hospital. Female CF-1 and Institute of Cancer Research severely combined immunodeficient (SCID) female mice (4–5 weeks of age) were supplied by Taconic Farms (Germantown, NY, USA). The mice were housed five animals per cage in sterile microisolator cages in a temperature- and humidity-controlled room with a 12-h light/12-h dark schedule. The animals were fed autoclaved rodent chow (Ralston Purina 300 Company, St. Louis, MO, USA) and water ad libitum. SCID mice were anesthetized for injections with isoflurane (Baxter Healthcare Corp., Deerfield, IL, USA) at a rate of 2.5% with 0.4 L oxygen through a nonrebreathing anesthesia vaporizer. PC-3 cells were injected into the bilateral subcutaneous flanks with ~5×10^6 PC-3 cells in a suspension of 100 μl normal sterile saline per injection site. Tumors were allowed to grow 2–3 weeks postinoculation, developing tumors ranging in mass from 0.03 to 0.28 g. Biodistribution studies were performed in CF-1 and SCID mice after tail vein injection with 750 kBq (~20 μCi) of ^{64}Cu-NO2A-RGD-Glu-6-Ahx-BBN(7-14)NH_2 in 100 μl of isotonic saline. CF-1 mice were humanely euthanized at 1 h p.i., and SCID mice were humanely euthanized at 1, 4 and 24 h p.i. Tissues and organs were excised from the animals and were weighed, along with urine, and the associated radioactivity was counted in a NaI well counter. The %ID and the %ID/g of each organ or tissue were calculated. The %ID in whole blood was estimated assuming a whole blood volume of 6.5% of the total body weight. Urine activity was reported as %ID and consisted of radioactivity in the urine, bladder and cage paper. The %ID/g of tumor tissue is reported as the average and standard deviation of the two individual bilateral xenografts.

2.5.2. MicroPET/micro-computed tomography (CT) imaging studies—Maximum intensity microPET coronal images were obtained on a Siemens INVEON small-animal, dedicated PET unit (Siemens, Nashville, TN, USA). The unit has a transverse field of view (FOV) of 10 cm and an axial length of 12.7 cm. The scanner operates in a three-dimensional (3D) volume imaging acquisition mode. Small animals were laser aligned at the center of the scanner FOV for subsequent imaging. Mice bearing xenografted human prostate PC-3 tumors were administered 26 MBq (700 μCi) of ^{64}Cu-NO2A-RGD-Glu-6-Ahx-BBN(7-14)NH_2 conjugate in 100 μl of isotonic saline via tail vein injection. At 15 h p.i., the mice were humanely euthanized by CO_2 administration. MicroPET image reconstruction

was obtained with an ordered subset expectation maximization algorithm with 3D resolution recovery and the absence of tissue attenuation correction. The microPET data were filtered with a Gaussian full width at half maximum filter. Additionally, the microCT coronal images were also obtained on the Siemens INVEON small-animal CT unit (Nashville, TN, USA) immediately after microPET for the purpose of anatomic/molecular data fusion. The microCT images were acquired for ~8 min, and concurrent image reconstruction was achieved using a cone beam (Feldkamp) filtered backprojection algorithm. The reconstructed (raw) microPET data sets (with a matrix size of 512×512×159) were imported into the Inveon Research Workstation software for subsequent image fusion with the microCT image data and 3D visualization.

3. Results

3.1. Chemistry and radiochemistry

NO2A-RGD-Glu-6-Ahx-BBN(7-14)NH_2 and ^{nat}Cu-NO2A-RGD-Glu-6-Ahx-BBN(7-14)NH_2 conjugates were synthesized in yields of ~70% and analyzed by RP-HPLC and MS to confirm their identity and purity (Table 1). The structure of ^{nat}Cu-NO2A-RGD-Glu-6-Ahx-BBN(7-14)NH_2 is shown in Fig. 1. The ^{64}Cu-labeled tracer eluted slightly faster than the unlabeled free peptide, with radiochemical purity >95% as determined by analytic radio-HPLC (Fig. 2).

3.2. In vitro assays

3.2.1. In vitro competitive cell binding assays—In vitro competitive cell binding assays of NO2A-RGD-Glu-6-Ahx-BBN(7-14)NH_2 and ^{nat}Cu-NO2A-RGD-Glu-6-Ahx-BBN(7-14)NH_2 conjugates were performed on human androgen-insensitive prostate cancer PC-3 cells that are known to express GRPrs in very high numbers. ^{125}I-[Tyr^4]-BBN was used as the displacement radioligand. Both the nonmetallated and metallated conjugates show very high binding affinity towards the GRPr, with IC_{50} values in the single-digit nanomolar range (Table 1, Fig. 3). In fact, the binding affinities for these new conjugates are similar to those reported for monomeric agonist conjugates of the type ^{nat}Cu-NO2A-X-BBN(7-14)NH_2, where X=AMBA, β-Ala, 5-Ava, 6-Ahx, 8-Aoc and 9-Anc, respectively [22]. On the other hand, the GRPr binding affinity of ^{nat}Cu-NO2A-RGD-Glu-6-Ahx-BBN(7-14)NH_2, as reported herein, appears to be superior to the nonmetallated NO3A-RGD-BBN(7-14)NH_2 (92.75±3.53 nM) targeting probe that has recently been reported by Liu and coworkers [14,18]. Differences in binding affinity could be merely the result of a metallated versus a nonmetallated species. However, there are subtle differences in chemical structures that exist between the two targeting vectors, and this may have some bearing on the differences in binding affinities for the GRPr as well. For example, in the study presented by Liu and coworkers, a triacetate *p*-NCS-Bz-NOTA chelating ligand was used to complex the radiometal and to covalently link to the peptide heterodimer. In the current study, the NOTA chelator lacks the *p*-NCS-Bz arm and forms an amide linkage via the third carboxylic acid unit of NOTA, resulting in a neutral conjugate upon binding to copper(II). From these results, it can clearly be determined that the complexing agent/metal complex has a definitive purpose for influencing the biodistribution of the radiopharmaceutical.

To probe the binding affinity of the RGD moiety for $\alpha_v\beta_3$ receptors on PC-3 cells, a sample of previously synthesized NO2A-RGD was reacted with $^{nat}CuCl_2$ as described above. Cell binding assays on the resultant ^{nat}Cu-NO2A-RGD complex revealed minimal displacement of ^{125}I-Echistatin, indicating minimal binding and very low affinity of monomeric RGD conjugate for $\alpha_v\beta_3$ receptors on PC-3 cells. Similarly, ^{nat}Cu-NO2A-RGD-Glu-6-Ahx-BBN(7-14)NH_2 showed minimal displacement of ^{125}I-Echistatin radioligand in PC-3 cells, indicating the primary driving force for cell binding to be GRPr mediated.

3.2.2. In vitro internalization studies—Internalization is the process of radioconjugate accumulation over time within the cells expressing the targeted receptors. The internalization behavior of the ^{64}Cu-NO2A-RGD-Glu-6-Ahx-BBN(7-14)NH_2 conjugate in human PC-3 prostate cancer cells was studied by incubation at 37°C for 15, 30, 45, 60, 90 and 120 min and characterized by a gradually increasing rate of accumulation within the cells. Internalization rates remained less than 1% for all time points surveyed. This is in stark contrast to monomeric ligands of similar structure, ^{nat}Cu-NO2A-X-BBN(7-14)NH_2, in which internalization rates of 1.5%–4.8% (relative of total radiotracer activity added to the well plate) were observed at a time point of 2 h postincubation [23]. In the current study, internalization reached a maximum at ~90 min postincubation (Fig. 4). It should also be noted that for conjugates of the general type ^{64}Cu-NO3A-RGD-BBN(7-14)NH_2 [18], internalization rates are approximately three times higher at later time points compared to the results for ^{64}Cu-NO2A-RGD-Glu-6-Ahx-BBN(7-14)NH_2, as presented herein. Differences between the chemical structures for each of the two targeting vectors could do much to influence the rate of internalization. A more plausible explanation, however, could simply be the method of calculation of the amount of radioactivity internalized. In the current study, we have opted to calculate the percent of internalization as a fraction of the total radioactivity added to the sample plate and not as a fraction of only cell-associated (surface plus internalized) radioactivity.

In a blocking experiment, neither nonradioactive BBN nor RGD could effectively inhibit cellular uptake of ^{64}Cu-NO2A-RGD-Glu-6-Ahx-BBN(7-14)NH_2. For example, blocking studies in which 50 μg of NO2A-6-Ahx-BBN(7-14) NH_2 was added to the cells 15 min prior to administration of ^{64}Cu-NO2A-RGD-Glu-6-Ahx-BBN(7-14)NH_2 reduced cellular uptake of tracer by approximately 61%. Administration of 50 μg of NO2A-RGD 15 min prior to addition of ^{64}Cu-NO2A-RGD-Glu-6-Ahx-BBN(7-14)NH_2 showed an ability to effectively block the tracer in PC-3 cells comparable to NO2A-6-Ahx-BBN(7-14)NH_2 (65%) and is very similar to previous in vivo investigations of similar ^{18}F-radiolabeled constructs [24].

3.3. In vivo assays

3.3.1. In vivo biodistribution studies in CF-1 mice—The biodistribution behavior of ^{64}Cu-NO2A-RGD-Glu-6-Ahx-BBN(7-14)NH_2 was studied in healthy CF-1 mice at 1 h p.i. to provide an initial assessment of its GRPr-targeting capability. The conjugate showed rapid and moderately high uptake (5.90±1.74%ID/g) at 1 h p.i. in normal pancreatic tissue, illustrating the effectiveness of this radioconjugate for targeting the GRPr. It is well known that the pancreas is the primary nonmalignant tissue expressing a high density of GRP cell-surface receptors in rodent models [8,25]. Liver retention was minimal (0.84±0.05%ID/g), illustrating high in vivo kinetic inertness and normal metabolic processes for excretion of conjugate. Rapid clearance from blood was also observed, with 0.42%ID remaining in circulation at 1 h p.i. The heterodimeric RGD-BBN radioligand also exhibited rapid urinary excretion, as nearly 85% was eliminated after 1 h p.i. ^{64}Cu-NO2A-RGD-Glu-6-Ahx-BBN(7-14)NH_2 conjugate demonstrated favorable pharmacokinetic properties for molecular imaging and was therefore chosen to be studied in PC-3 tumor-bearing SCID mice.

3.3.2. In vivo biodistribution studies in PC-3 tumor-bearing mice—A summary of the biodistribution data (1, 4 and 24 h p.i.) for ^{64}Cu-NO2A-RGD-Glu-6-Ahx-BBN(7-14)NH_2 conjugate administered to SCID mice bearing PC-3 xenografts (n=5 for each time point) is shown in Table 2 and Fig. 5. Again, the conjugate cleared effectively from the bloodstream, with 0.72±0.10%ID remaining at 1 h p.i. The main excretion route, as was also observed for normal CF-1 mice, occurred primarily through the renal–urinary system. Minimal accumulation of radioactivity was observed in the liver at all three time

points, ranging from 1.04±0.08%ID/g at 1 h p.i. to 1.24±0.23%ID/g at 24 h p.i. This again validates results from our previous studies demonstrating the effective kinetic stability of the Cu(II)-NO2A metal complex under in vivo conditions [8]. Moderately high uptake (3.96±1.04%ID/g) of radiotracer was observed in the tumors at 1 h p.i., of which ~60% of the radioactivity was retained at 24 h p.i. In contrast to the prolonged retention of radiotracer in the tumor tissue, rapid clearance of the conjugate was observed for all other tissues. Considerably high pancreatic uptake (21.65±3.30%ID/g) was observed at 1 h p.i. Reduction of pancreatic accumulation by ~76% was observed at 24 h p.i. (5.18±0.57%ID/g).

3.3.3. Tumor/nontumor uptake ratios—The major pharmacokinetic consideration in the development of peptide-based imaging agents is to achieve a diagnostically useful tumor/nontumor uptake ratio. The tumor/nontumor ratios for ^{64}Cu-NO2A-RGD-Glu-6-Ahx-BBN(7-14)NH_2 are shown in Table 3 at 1, 4 and 24 h p.i. High and diagnostically useful tumor/nontumor uptake ratios were achieved in most of the tissues after 1 and 4 h p.i. The tumor/nontumor uptake values were significantly high for certain tissues (muscle and bone) at all times points. Lower tumor/nontumor ratios observed for small intestine (1 h), large intestine (4 h) and pancreas (all time points) corroborate the fact that these organs express the GRPr and that a small amount of injected conjugate is metabolized in the gastrointestinal tract. It was clear from the tumor/nontumor uptake ratios that diagnostically useful ratios could be achieved in most of the abdominal tissues after a substantial delayed time point, which led us to perform the microPET/CT imaging study at 15 h p.i.

3.3.4. MicroPET/CT imaging studies—MicroPET imaging studies of ^{64}Cu-NO2A-RGD-Glu-6-Ahx-BBN(7-14)NH_2 conjugate in a PC-3 tumor-bearing mouse at 15 h p.i. (Fig. 6) produced high-quality, high-contrast images and provide some impetus for this heterodimeric RGD-BBN agonist conjugate to be potentially used as a site-directed PET targeting agent for primary or metastatic prostate cancer in human patients. Briefly, 26 MBq (700 μCi) of conjugate was administered to a tumor-bearing rodent via the tail vein. At 15 h p.i., the mouse was humanely euthanized, and subsequent imaging studies were performed. The radioactivity distribution and retention in the microPET/CT images are consistent with the biodistribution data obtained from the in vivo pharmacokinetic assays. Virtually no accumulation of radioactivity in the gastrointestinal tract suggests rapid clearance of the conjugate from collateral tissue primarily via the renal–urinary tract.

4. Discussion

In recent years, our group and many others have focused upon the development of ^{64}Cu-labeled monomeric BBN analogs for targeting specific human cancers. ^{64}Cu-labeled BBN(7-14)NH_2 radiopharmaceuticals have been of interest due to the ideal nuclear characteristics of Cu-64, ^{64}Cu [$t_{1/2}$=12.7 h; Eβ+$_{max}$=0.65 MeV (17.9%); Eβ$^-_{max}$=0.57 MeV (39%); electron capture (43.1%)], making it useful for in vivo molecular imaging. The half-life for ^{64}Cu is sufficiently long enough for drug preparation, quality control, drug incorporation, circulation and patient imaging/therapy. Copper-64 has become more popular as its availability increases. Not only does it possess ideal characteristics for PET imaging, but it engages in straightforward substitution chemistry and forms stable complexes as a copper(II) cation [8,26,27]. For example, recent studies have demonstrated that ligands of the CB-TE2A, NO2A and sarcophagine variety form thermodynamically stable and kinetically inert complexes with copper(II) cation.

In this study, we have presented the synthesis, characterization and biological behavior of a neutral heterodimeric conjugate of the formula ^{64}Cu-NO2A-RGD-Glu-6-Ahx-BBN(7-14)NH_2 for dual receptor targeting in PC-3 cells. The NOTA bifunctional chelator effectively stabilizes copper(II) in vivo and reduces dissociation and transchelation of the

metal, minimizing hepatobiliary uptake and excretion via the gastrointestinal tract. It is superior to DOTA-based chelators in terms of kinetic stability and is much easier to radiolabel and synthesize than CB-TE2A [8,18]. NOTA chelator, for example, can be radiolabeled at room temperature [22]. Our conjugate that is presented herein is very similar to a previous study that reported an anionic, heterodimeric RGD-BBN molecule. The authors employed a NOTA derivative with a *p*-NCS-Bz arm linking the peptide to the chelator. This strategy frees one of the carboxylic acid units (two are still used to bind to copper), creating an anionic complex (radiolabeling occurs at slightly basic pH). Our NOTA chelator lacks the *p*-NCS-Bz arm and forms an amide linkage via the third carboxylic acid unit, resulting in a neutral conjugate upon binding to copper(II), which may overcome prolonged retention in renal tissue to produce very high quality microPET images. Additionally, the presence of *p*-NCS-Bz might alter the pharmacokinetic properties of the conjugate. For example, liver uptake of the ^{64}Cu-NO3A-RGD-BBN(7-14)NH_2 anionic probe was 2.80±1.15%ID/g at 1 h compared to 1.04±0.08%ID/g for our molecule [18]. One of our initial hypotheses was that our neutral conjugates would exhibit lower kidney uptake values than the anionic analogues [18]. Surprisingly, our biodistribution data at 1 h p.i. in tumor-bearing SCID mice (4.65±0.78%ID/g) show higher kidney uptake values than Liu's compound (3.06±0.25%ID/g). However, at 24 h p.i., kidney retention diminished to 1.20±0.36%ID/g (compared to 1.87±0.41%ID/g at 20 h p.i. for the anionic analog), demonstrating sufficient clearance from the renal–urinary tract.

High retention of radioconjugate in tumor tissue may be due in part to the fact that the human tumor xenografts are supported by murine vasculature architecture [28]. On the other hand, the low retention of radioconjugate in pancreatic tissue may be due in part to excessive enzymatic activity of the pancreatic tissue [29]. The high uptake and retention in PC-3 tumor cells are a direct reflection of the efficiency of agonist-based constructs for in vivo targeting of the GRP cell surface receptors. Although our conjugate exhibited higher initial tumor uptake at 1 h (3.95±1.04%ID/g) than Liu's (2.78±0.56%ID/g), both conjugates retained much of their tumor-associated radioactivity several hours after injection. Perhaps the RGD motif plays a supplementary post facto role in binding, engaging with the $\alpha_v\beta_3$ receptor after initial binding of the BBN(7-14)NH_2 fragment with the GRPr occurs, thus enhancing retention of the radiopharmaceutical in the cell. It should be noted, however, that simultaneous binding of the RGD and BBN sequences does *not* occur [11].

Previous studies have concluded that heterodimeric ^{64}Cu-NO3A-RGD-BBN(7-14)NH_2 provided better results than monomeric ^{64}Cu-NO3A-RGD and ^{64}Cu-NO3A-BBN(7-14)NH_2 in terms of biodistribution data and PET imaging. Indeed, it appears that the RGD and BBN targeting motifs alone perform more poorly than when in tandem. Here we have focused primarily on the neutral heterodimeric ^{64}Cu-NO2A-RGD-Glu-6-Ahx-BBN(7-14)NH_2 conjugate rather than ^{64}Cu-NO2A-6-Ahx-BBN(7-14)NH_2 and/or ^{64}Cu-NO2A-RGD, thus opting for a direct comparison to the anionic ^{64}Cu-NO3A-RGD-BBN(7-14)NH_2 analogue from an earlier study [18]. Fig. 7, however, demonstrates the effectiveness of retention in GRPr-expressing tissues for heterodimeric ^{64}Cu-NO2A-RGD-Glu-6-Ahx-BBN(7-14)NH_2 as compared to monomeric ^{64}Cu-NO2A-6-Ahx-BBN(7-14)NH_2 [23] conjugate in the same animal model. A Student's *t* test (24 h p.i.) in GRPr-expressing pancreas and tumor produced *P* values of .0019 and .0015, respectively, indicating statistical significance between the four data sets at the 95% confidence interval. Retention in liver, although not statistically significant (*P* value=.33 at the 95% confidence interval), appears to be lower for the heterodimeric ^{64}Cu-NO2A-RGD-Glu-6-Ahx-BBN(7-14)NH_2 as compared to monomeric ^{64}Cu-NO2A-6-Ahx-BBN(7-14)NH_2. MicroPET molecularimaging investigations clearly support the in vivo biodistribution investigations as presented herein.

We also believe the BBN targeting vector to be the workhorse in terms of initial binding to PC-3 cell surface receptors. Single-digit IC_{50} values in the nanomolar range reflect a high degree of binding affinity of the BBN(7-14)NH_2 fragment for the GRPr [NO2A-RGD-Glu-6-Ahx-BBN(7-14) NH_2 and ^{nat}Cu-NO2A-RGD-Glu-6-Ahx-BBN(7-14) NH_2=3.99±0.35 and 8.98±1.34 nM, respectively]. In vitro binding studies of ^{nat}Cu-NO2A-RGD and ^{nat}Cu-NO2A-RGD-Glu-6-Ahx-BBN(7-14)NH_2 for $\alpha_v\beta_3$ receptors expressed on PC-3 cells showed extremely poor binding affinity, authenticating the fact that the BBN targeting motif is responsible for binding the radioconjugate to the PC-3 tumor cell [18]. However, we do believe that the RGD sequence facilitates tumor accumulation, retention and renal–urinary excretion, although it plays only a minimal role in initial binding of tracer. The heterodimeric conjugate ^{64}Cu-NO2A-RGD-Glu-6-Ahx-BBN(7-14)NH_2 showed favorable biodistribution properties for molecular imaging, specifically with tumor retention and organs housed along the gastrointestinal tract. High-quality, high-contrast PET images of PC-3 tumors in a SCID mouse were obtained using the ^{64}Cu-NO2A-RGD-Glu-6-Ahx-BBN(7-14)NH_2 radioligand reported herein. This first example of a neutral, heterodimeric, RGD-BBN agonist radioconjugate prepared in our laboratory definitely confers enough evidence to further investigate additional analogs using variations of the pharmacokinetic modifier (6-Ahx in this case) and/or bifunctional chelator for pharmacokinetic optimization and subsequent comparative PET imaging studies.

5. Conclusion

Until now, many of the studies toward development of site-directed molecular imaging agents have focused upon the pharmacokinetic modifier or the targeting vector for fine tuning the in vivo behavior of the tracer. ^{64}Cu-NO2A-RGD-Glu-6-Ahx-BBN(7-14)NH_2, as reported herein, differs from ^{64}Cu-NO3A-RGD-BBN(7-14)NH_2 [18] by approximately 170 atomic mass units. Yet, the pharmacokinetics and microPET molecular images of each conjugate are strikingly dissimilar. Studies in our laboratory and many others have indicated that only subtle differences in the pharmacokinetic modifier can have a rather large influence on the pharmacokinetics of the tracer. Furthermore, as previously indicated, there are numerous complexing agents that have produced stable conjugates with ^{64}Cu radiometal. CB-TE2A, NO2A, NO3A and sarcophagine ligand frameworks form thermodynamically stable and kinetically inert complexes with copper(II) cation. However, each of the four ligand types tend to produce altogether different biodistributions with similar targeting vectors [25]. Clearly, from the studies reported herein, the complexing agent/metal complex also has a definitive purpose for influencing the biodistribution of the radiopharmaceutical. For effective site-directed diagnostic or therapeutic agents, it is essential to find those pieces of the puzzle that produce optimum target uptake and retention with little or no background radiation in collateral tissues. In other words, a complexing agent or pharmacokinetic modifier that produces ideal results with a given targeting vector such as bombesin can be altogether ineffective with other peptides such as somatostatin or melanotropin.

Herein, we have reported the synthesis, characterization and biological evaluation of ^{64}Cu-NO2A-RGD-Glu-6-Ahx-BBN(7-14)NH_2, a neutral, heterodimeric conjugate for specific targeting of the GRPr on human prostate PC-3 tumor cells using in vitro assays, in vivo biodistribution assays and microPET/CT molecular imaging studies. This conjugate exhibited high accumulation in GRPr-expressing tissue and efficient clearance of radiotracer from whole-body tissue via the renal–urinary excretion pathway. Molecular imaging studies produced excellent microPET images in a PC-3 tumor-bearing mouse, suggesting that this and analogous heterodimeric RGD-BBN conjugates could be used as peptide-based PET tracer agonists for the diagnosis of GRPr-positive tumors in human patients.

Acknowledgments

This material was the result of work supported with resources and the use of facilities at the Harry S. Truman Memorial Veterans' Hospital, Columbia, MO 65201, and the University of Missouri School of Medicine, Columbia, MO 65211, USA. This work was funded in part by The United States Department of Veterans' Affairs VA Merit Award.

References

1. Behr TM, Gotthardt M, Barth A, Béhé M. Imaging tumors with peptide-based radioligands. Q J Nucl Med. 2001; 45:189–200. [PubMed: 11476170]
2. Blum JE, Handmaker H. Small peptide radiopharmaceuticals in the imaging of acute thrombus. Curr Pharm Des. 2002; 8:1815–26. [PubMed: 12171533]
3. Krenning EP, De Jong M. Therapeutic use of radiolabelled peptides. Ann Oncol. 2000; 11:267–71. [PubMed: 11079151]
4. Krenning EP, Kwekkeboom DJ, Valkema R, Pauwels S, Kvols LK, De Jong M. Peptide receptor imaging and therapy. Ann N Y Acad Sci. 2004; 1014:234–45. [PubMed: 15153440]
5. Liu S, Edwards DS. ^{99m}Tc-labeled small peptides as diagnostic radiopharmaceuticals. Chem Rev. 1999; 99:2235–68. [PubMed: 11749481]
6. Markwalder R, Reubi JC. Gastrin-releasing peptide receptors in the human prostate: relation to neoplastic transformation. Cancer Res. 1999; 59:1152–9. [PubMed: 10070977]
7. Okarvi SM. Recent progress in fluorine-18 labelled peptide radiophar-maceuticals. Eur J Nucl Med. 2001; 28:929–38. [PubMed: 11504093]
8. Prasanphanich AF, Nanda PK, Rold TL, Ma L, Lewis MR, Garrison JC, et al. [^{64}Cu-NOTA-8-Aoc-BBN(7-14)NH_2] targeting vector for positron-emission tomography imaging of gastrin-releasing peptide receptor-expressing tissues. Proc Nat Acad Sci U S A. 2007; 104:12462–7.
9. Signore A, Annovazzi A, Chianelli M, Corsetti F, Van de Wiele C, Watherhouse RN. Peptide radiopharmaceuticals for diagnosis and therapy. Eur J Nucl Med. 2001; 28:1555–65. [PubMed: 11685500]
10. Smith CJ, Volkert WA, Hoffman TJ. Radiolabeled peptide conjugates for targeting of the bombesin receptor superfamily subtypes. Nucl Med Biol. 2005; 32:733–40. [PubMed: 16243649]
11. Chen K, Conti PS. Target-specific delivery of peptide-based probes for PET imaging. Adv Drug Deliv Rev. 2010; 62:1005–22. [PubMed: 20851156]
12. Lee S, Xie J, Chen X. Peptides and peptide hormones for molecular imaging and disease diagnosis. Chem Rev. 2010; 110:3087–111. [PubMed: 20225899]
13. Liu S. Radiolabeled heterodimeric cyclic RGD peptides as integrin $\alpha_v\beta_3$ targeted radiotracers for tumor imaging. Mol Pharm. 2006; 3:472–87. [PubMed: 17009846]
14. Liu S. Radiolabeled cyclic RGD peptides as integrin $\alpha_v\beta_3$-targeted radiotracers: maximizing binding affinity via bivalency. Bioconjug Chem. 2009; 20:2199–213. [PubMed: 19719118]
15. Schottelius M, Laufer B, Kessler M, Wester MS. Ligands for mapping $\alpha_v\beta_3$-integrin expression in vivo. Acc Chem Res. 2009; 42:969–80. [PubMed: 19489579]
16. Liu Z, Wang F. Dual targeted molecular probes for cancer imaging. Curr Pharm Biotechnol. 2010; 11:610–9. [PubMed: 20497116]
17. Li ZB, Chen K, Chen X. ^{68}Ga-labeled heterodimeric RGD peptides for microPET imaging of integrin $\alpha_v\beta_3$ expression. Eur J Nucl Med Mol Imaging. 2008; 35:1100–8. [PubMed: 18204838]
18. Liu Z, Li ZB, Cao Q, Liu S, Wang F, Chen X. Small-animal PET of tumors with ^{64}Cu-labeled RGD-bombesin heterodimer. J Nucl Med. 2009; 50:1168–77. [PubMed: 19525469]
19. Liu Z, Niu G, Wang F, Chen X. ^{68}Ga-labeled NOTA-RGD-BBN peptide for dual integrin and GRPR-targeted tumor imaging. Eur J Nucl Med Mol Imaging. 2009; 36:1483–94. [PubMed: 19360404]
20. Liu Z, Yan Y, Liu S, Wang F, Chen X. ^{18}F, ^{64}Cu, and ^{68}Ga labeled RGD-bombesin heterodimeric peptides for PET imaging of breast cancer. Bioconjug Chem. 2009; 20:1016–25. [PubMed: 20540537]

21. Wu Y, Zhang X, Xiong Z, Cheng Z, Fisher DR, Liu S, et al. microPET imaging of glioma integrin $\alpha_v\beta_3$ expression using ^{64}Cu-labeled tetrameric RGD peptide. J Nucl Med. 2005; 46:1707–18. [PubMed: 16204722]
22. Prasanphanich AF, Retzloff L, Lane SR, Nanda PK, Sieckman GL, Rold TL, et al. In vitro and in vivo analysis of [^{64}Cu-NO2A-8-Aoc-BBN(7-14)NH_2]: a site-directed radiopharmaceutical for positron-emission tomography imaging of T-47D human breast cancer tumors. Nucl Med Biol. 2009; 36:171–81. [PubMed: 19217529]
23. Lane SR, Nanda P, Rold TL, Sieckman GL, Figueroa SD, Hoffman TJ, et al. Optimization, biological evaluation and microPET imaging of copper-64-labeled bombesin agonists, [^{64}Cu-NO2A-(X)-BBN(7-14) NH_2], in a prostate tumor xenografted mouse model. Nucl Med Biol. 2010; 37:751–61. [PubMed: 20870150]
24. Li ZB, Wu Z, Chen K, Ryu EK, Chen X. 18F-labeled BBN-RGD heterodimer for prostate cancer imaging. J Nucl Med. 2008; 49:453–61. [PubMed: 18287274]
25. Hoffman TJ, Smith CJ. True radiotracers: Cu-64 targeting vectors based upon bombesin peptide. Nucl Med Biol. 2009; 36:579–85. [PubMed: 19647163]
26. Wadas TJ, Anderson CJ. Radiolabeling of TETA- and CB-TE2A-conjugated peptides with copper-64. Nat Protoc. 2007; 1:3062–8. [PubMed: 17406569]
27. Ma MT, Cooper MS, Paul RL, Shaw KP, Karas JA, Scanlon D, et al. Macrobicyclic cage amine ligands for copper radiopharmaceuticals: a single bivalent cage amine containing two Lys^3-bombesin targeting peptides. Inorg Chem. 2011; 50:6701–10. [PubMed: 21667932]
28. Hoffman TJ, Gali H, Smith CJ, Sieckman GL, Hayes DL, Owen NK, et al. Novel series of ^{111}In-labeled bombesin analogs as potential radiopharmaceuticals for specific targeting of gastrin-releasing peptide receptors expressed on human prostate cancer cells. J Nucl Med. 2003; 44:823–31. [PubMed: 12732685]
29. Nock B, Nikolopoulou A, Chiotellis E, Loudos G, Maintas D, Reubi JC, et al. ^{99m}Tc demobesin 1, a novel potent bombesin analogue for GRP receptor-targeted tumour imaging. Eur J Nucl Med Mol Imaging. 2003; 30:247–58. [PubMed: 12552343]

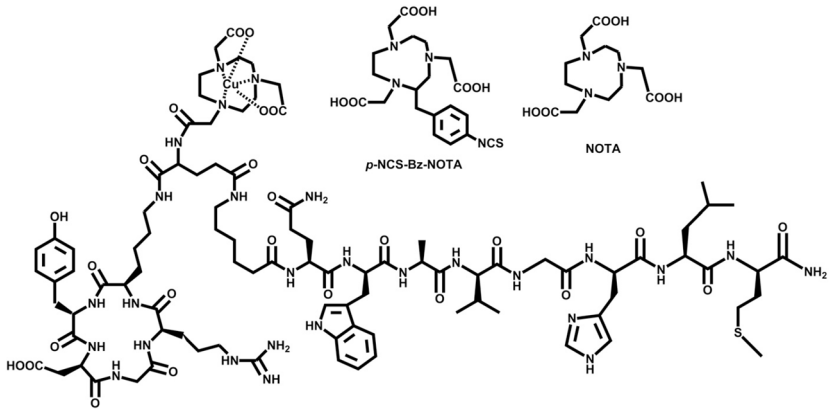

Fig. 1.

Chemical representations of *p*-NCS-Bz-NOTA (NO3A) [18] and NOTA bifunctional chelators and the structure of ^{nat}Cu-NO2A-RGD-Glu-6-Ahx-BBN(7-14)NH_2 conjugate.

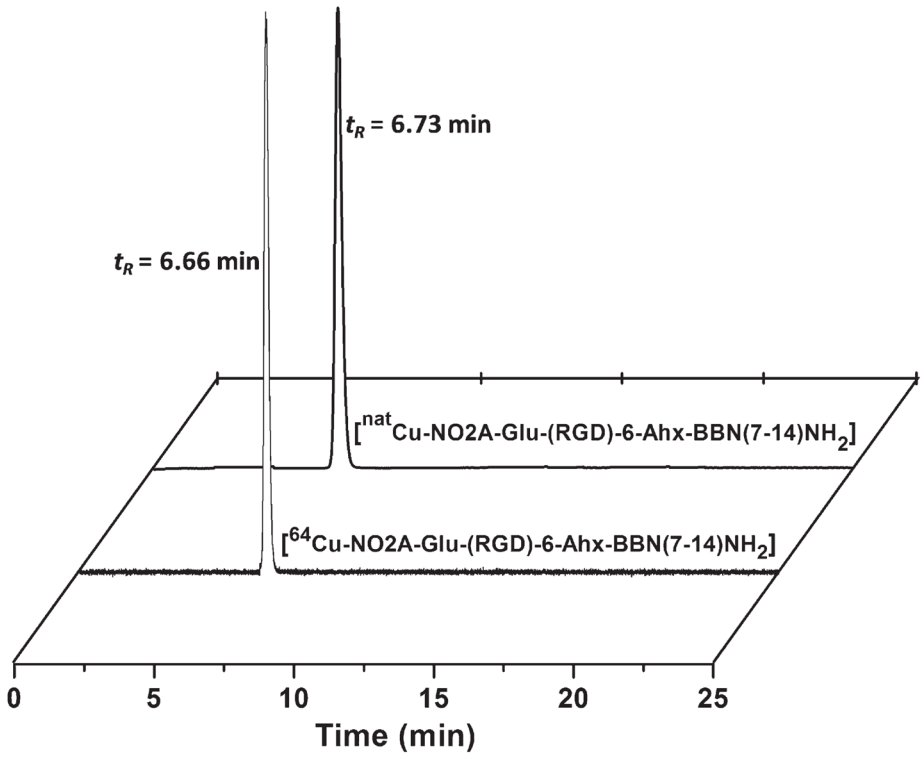

Fig. 2.

HPLC chromatographic profiles of ^{nat}Cu-NO2A-RGD-Glu-6-Ahx-BBN(7-14)NH$_2$ (t_R=6.73 min) and ^{64}Cu-NO2A-RGD-Glu-6-Ahx-BBN(7-14)NH$_2$ (t_R=6.66 min).

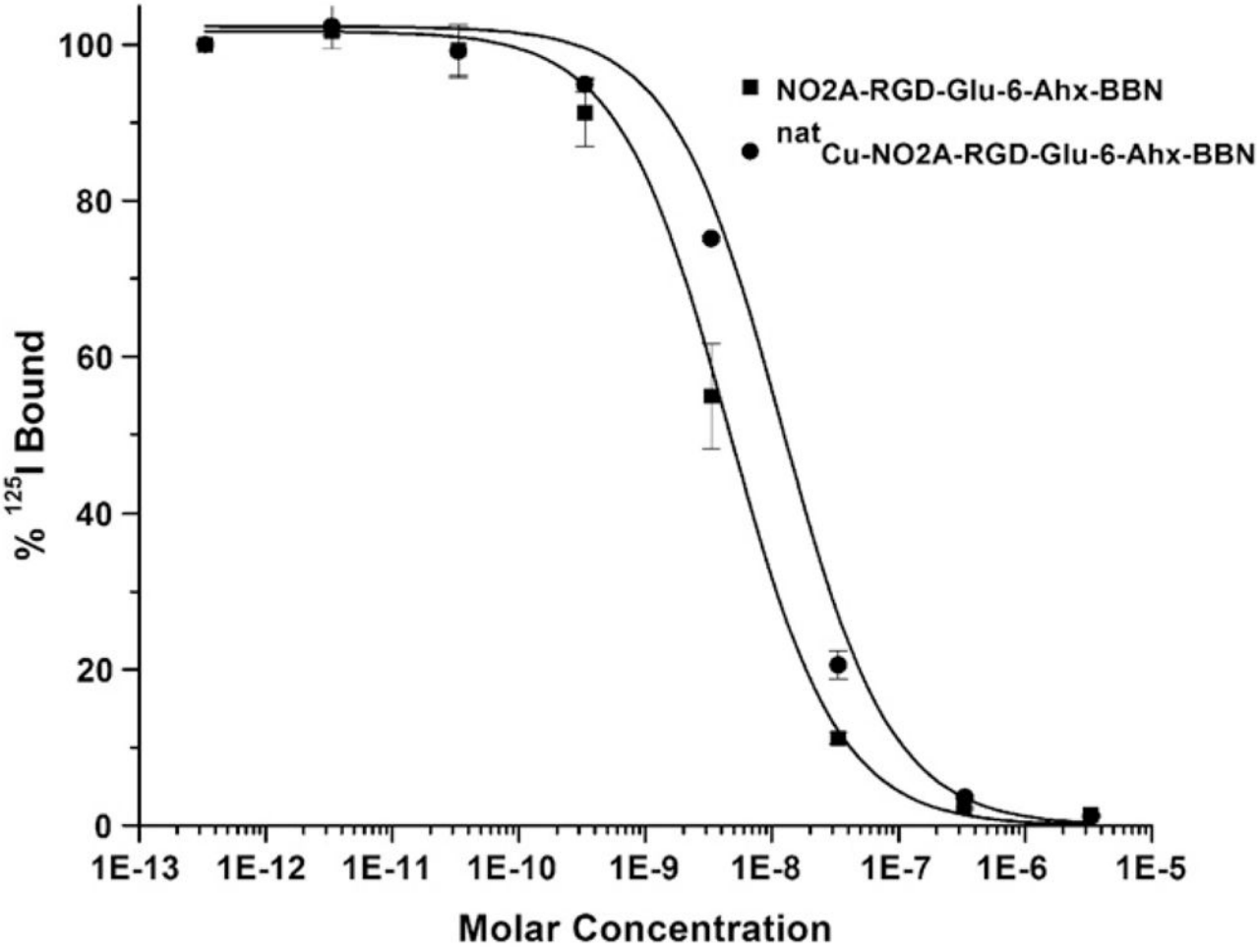

Fig. 3.

Inhibitory concentration half maximum (IC_{50}) of NO2A-RGD-Glu-6-Ahx-BBN(7-14)NH_2 (IC_{50}=3.99±0.35 nM) and ^{nat}Cu-NO2A-RGD-Glu-6-Ahx-BBN(7-14)NH_2 (IC_{50}=8.98±1.34 nM).

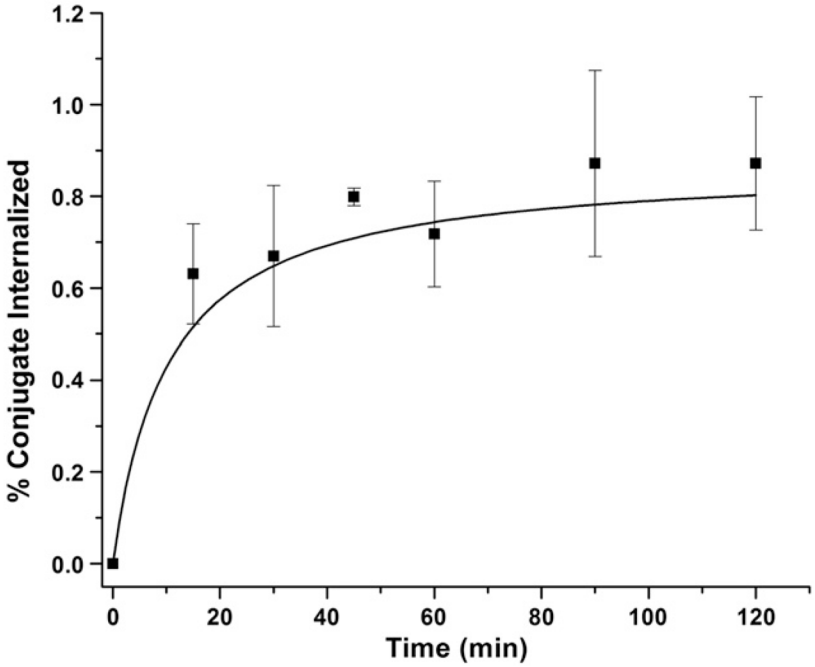

Fig. 4.
Internalization data for ^{64}Cu-NO2A-RGD-Glu-6-Ahx-BBN(7-14) NH_2 in human, PC-3 prostate tumor cells.

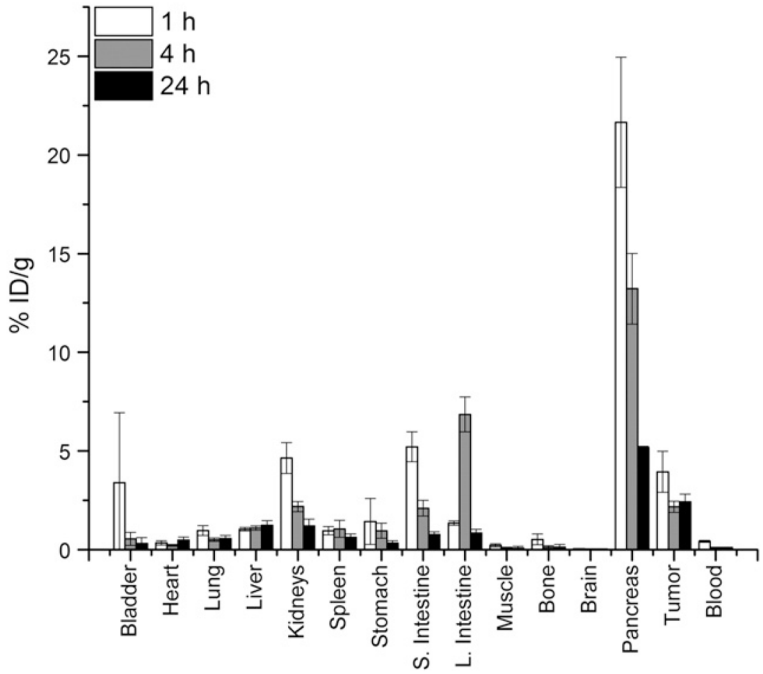

Fig. 5.
Biodistribution data of ^{64}Cu-NO2A-RGD-Glu-6-Ahx-BBN(7-14)NH_2 in PC-3 tumor-bearing SCID mice at 1, 4 and 24 h p.i.

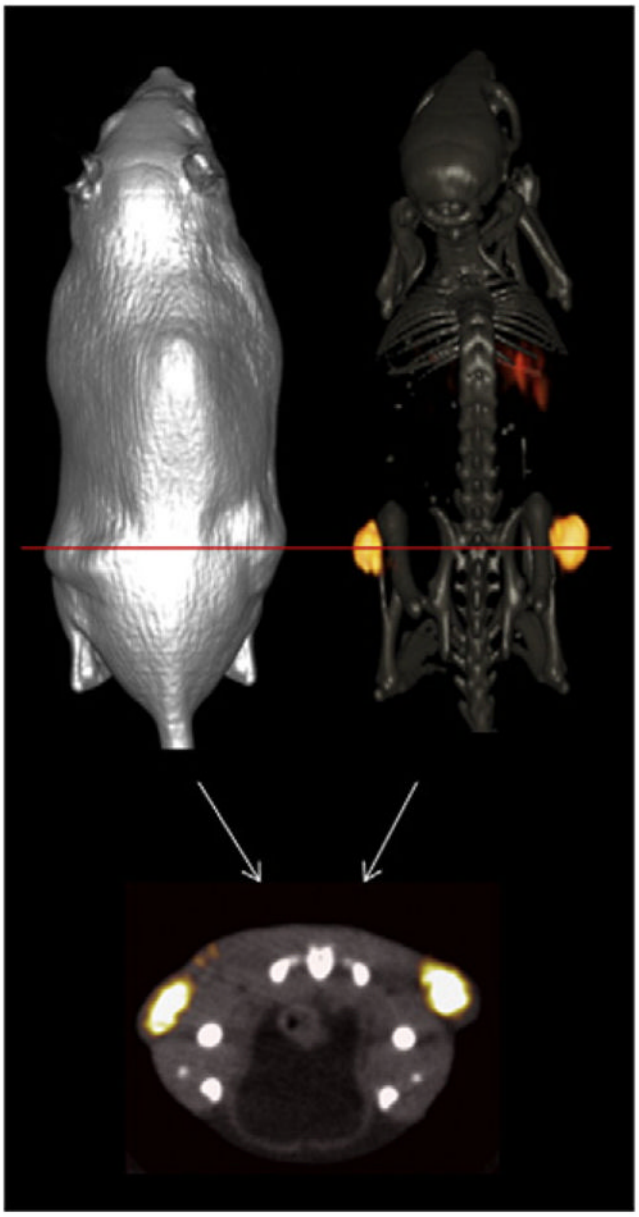

Fig. 6.

Maximum-intensity microPET tumor and microCT skeletal fusion coronal whole-body image (right) and soft tissue image (left) of a PC-3 tumor-bearing SCID mouse at 15 h after tail vein injection of ^{64}Cu-NO2A-RGD-Glu-6-Ahx-BBN(7-14)NH_2. Axial fused microPET/CT image shown below.

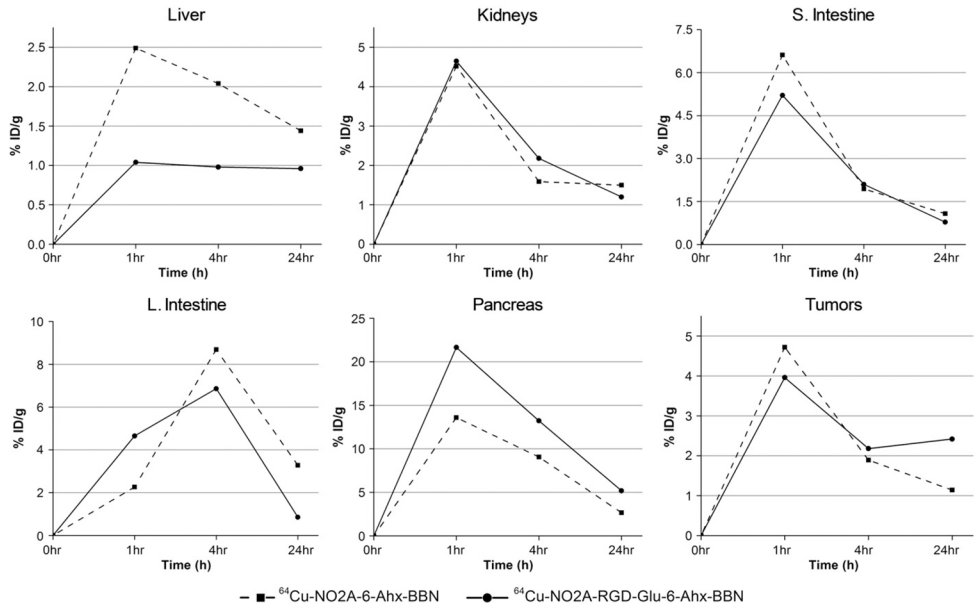

Fig. 7.

Biodistribution data of ^{64}Cu-NO2A-RGD-Glu-6-Ahx-BBN(7-14)NH_2 and ^{64}Cu-NO2A-6-Ahx-BBN(7-14)NH_2 in specific tissue/organs (liver, kidneys, intestines, pancreas and tumor) of PC-3 tumor-bearing SCID mice at 1, 4 and 24 h p.i.

Table 1

Salient characterization data for NO2A-RGD-Glu-6-Ahx-BBN(7-14)NH_2 conjugate

Calculated molecular mass, kDa	2069.35
Calculated molecular mass, kDa (^{nat}Cu)	2130.88
Electrospray ionization molecular mass, kDa	2070.41
Electrospray ionization molecular mass, kDa (^{nat}Cu)	2130.77
Formula	$C_{93}H_{141}N_{27}O_{25}S$
Formula (^{nat}Cu)	$C_{93}H_{139}N_{27}O_{25}SCu$
HPLC t_R, min	6.73
HPLC t_R, (^{64}Cu) min	6.66
IC_{50}, nM	3.99±0.35
IC_{50}, (^{nat}Cu) nM	8.98±1.34

Table 2

Biodistribution data of ^{64}Cu-NO2A-RGD-Glu-6-Ahx-BBN(7-14)NH_2 in PC-3 tumor-bearing SCID mice 1, 4 and 24 h p.i. (%ID/g±S.D., n=5)

Tissue	1 h	4 h	24 h
Bladder	3.39±3.54	0.55±0.33	0.31±0.29
Heart	0.35±0.10	0.22±0.05	0.48±0.17
Lung	0.97±0.25	0.51±0.08	0.56±0.16
Liver	1.04±0.08	1.10±0.11	1.24±0.23
Kidneys	4.65±0.78	2.18±0.26	1.20±0.36
Spleen	0.96±0.21	1.06±0.43	0.63±0.17
Stomach	1.43±1.16	0.96±0.39	0.34±0.12
Small intestine	5.21±0.75	2.10±0.40	0.78±0.14
Large intestine	1.34±0.11	6.86±0.88	0.85±0.18
Muscle	0.22±0.08	0.09±0.04	0.08±0.10
Bone	0.52±0.27	0.13±0.08	0.13±0.15
Brain	0.05±0.01	0.04±0.02	0.03±0.02
Pancreas	21.65±3.30	13.22±1.79	5.18±0.57
Tumor	3.96±1.36	2.18±0.31	2.42±0.57
Blood[a]	0.72±0.10	0.16±0.05	0.18±0.02
Excretion[a]	70.17±45.21	82.64±71.29	90.69±3.71

[a]Data presented as %ID.

Table 3

Target-to-nontumor uptake ratios of ^{64}Cu-NO2A-RGD-Glu-6-Ahx-BBN(7-14)NH_2 in PC-3 tumor-bearing SCID mice at 1, 4 and 24 h

Tissue	1 h	4 h	24 h
Blood	9.21	21.80	22.00
Liver	3.81	1.98	1.95
Kidneys	0.85	1.00	2.02
Small intestine	0.76	1.04	3.10
Large intestine	2.95	0.32	2.85
Muscle	18.00	24.22	30.25
Bone	7.61	16.76	18.61
Pancreas	0.18	0.16	0.47